Journal of Solid State Chemistry 181 (2008) 2763–2767

Contents lists available at ScienceDirect

Journal of Solid State Chemistry

journal homepage: www.elsevier.com/locate/jssc

Novel rare earth ions-doped oxyfluoride nano-composite with efficient upconversion white-light emission

Daqin Chen, Yuansheng Wang *, Yunlong Yu, Ping Huang, Fangyi Weng

State Key Laboratory of Structural Chemistry, Fujian Institute of Research on the Structure of Matter, Chinese Academy of Sciences, Fuzhou, Fujian 350002, PR China

ARTICLE INFO

Article history:
Received 28 May 2008
Received in revised form
2 July 2008
Accepted 6 July 2008
Available online 11 July 2008

Keywords:
Nano-composite
Crystallization
Optical materials
Luminescence

ABSTRACT

Transparent SiO_2–Al_2O_3–NaF–YF_3 bulk nano-composites triply doped with Ho^{3+}, Tm^{3+} and Yb^{3+} were fabricated by melt-quenching and subsequent heating. X-ray diffraction and transmission electron microscopy measurements demonstrated the homogeneous precipitation of the β-YF_3 crystals with mean size of 20 nm among the glass matrix, and rare earth ions were found to partition into these nano-crystals. Under single 976 nm laser excitation, intense red, green and blue upconversion emissions were simultaneously observed owing to the successive energy transfer from Yb^{3+} to Ho^{3+} or Tm^{3+}. Various colors of luminescence, including bright perfect white light, can be easily tuned by adjusting the concentrations of the rare earth ions in the material. The overall energy efficiency of the white-light upconversion was estimated to be about 0.2%.

1. Introduction

Infrared-to-visible frequency upconversion (UC) in rare earth (RE)-doped materials has been extensively investigated owing to its potential applications in UC lasers, high-density memories, solid-state color displays and other photonic devices [1–5]. For color displays, it is necessary to generate simultaneously the controllable red, green and blue (RGB) emissions. Indeed, there have been some reports on the control of luminescence in three primary colors through UC and the generation of white light. For example, Downing et al. [6] realized a three-dimensional solid-state display from fluoride glasses triply doped with Tm^{3+}, Er^{3+} and Pr^{3+} using three different pairs of near-infrared laser excitation sources. Despite the fact that the multiple pump wavelength configuration produces higher UC efficiencies, a single-pump scheme is mostly desired. Recently, RGB UC emissions and white-light simulation were achieved in some RE-doped materials under single infrared laser excitation [7–13]. However, the hosts were limited mainly in the fluoride and tellurite glasses.

As a novel optical material, the nano-structured transparent oxyfluoride glass ceramics have been extensively investigated in recent years for its low phonon energy of the fluoride nano-crystals and high mechanical, chemical stabilities of the amorphous oxide matrix. The key factor for the efficient luminescence is the abundant partition of the optically active RE ions into the precipitated fluoride nano-crystals [14–20]. In this work, the β-YF_3 nano-crystals embedded glass ceramics triply doped with Ho^{3+}, Tm^{3+} and Yb^{3+} were successfully prepared. The RE ions were found to partition into the precipitated fluoride nano-crystals with low phonon energy after crystallization. Under a single-pump scheme, the controllable RGB emissions and bright white-light generation through UC were realized in this nano-composite with appropriate RE doping.

2. Experimental details

The precursor glasses with the composition of $44SiO_2$–$28Al_2O_3$–$17NaF$–$11YF_3$ (in mol%) were prepared by melt quenching and subsequent heating. The RE doping was introduced by the addition of RE fluorides (HoF_3, TmF_3 and YbF_3) to the system. The glasses were prepared by melting a mixture of reagent grade chemical compositions in platinum crucible at 1400 °C for 30 min in the ambient atmosphere. The melt was poured into a 300 °C pre-heated copper mold and then allowed to cool to room temperature. The obtained bulk glasses were then cut into 5 mm^2 square coupons and heat-treated at 670 °C determined by the differential thermal analysis (DTA) measurement for 2 h to proceed crystallization of the fluoride nano-phase. All the nano-composites were highly transparent in the visible region.

To identify the crystallization phase, X-ray diffraction (XRD) analysis was carried out with a powder diffractometer (DMAX2500 RIGAKU) using Cu$K\alpha$ radiation ($\lambda = 0.154$ nm). The microstructures of the samples were studied using a transmission electron microscope (TEM, JEM-2010) equipped with an

* Corresponding author. Fax: +86 591 8370 5402.
E-mail address: yswang@fjirsm.ac.cn (Y. Wang).

0022-4596/$ - see front matter © 2008 Elsevier Inc. All rights reserved.
doi:10.1016/j.jssc.2008.07.003

energy-dispersive X-ray (EDX) spectroscopy system. The absorption spectra were measured on a spectrophotometer (Lambda 900, Perkin-Elmer) with a spectral range from 200 to 2000 nm and a resolution of 1.0 nm. The room temperature UC emission spectra were recorded using a Hamamatsu R943-02 photomultiplier tube and a Spex 1000 M monochromator under 976 nm Tsunami Ti:sapphire laser excitation. The pulse duration, energy and intensity of the Ti:sapphire laser are 2 ps, 15 nJ and 200 W/cm^2, respectively. The pump laser beam was focused onto the sample and the luminescence signal was collected in the direction perpendicular to the pump beam in order to avoid the disturbing of the scattered laser. In order to measure the absolute UC white-light power, a spectroradiometer (Topcon SR3) was used to collect the emission intensity and the signal obtained was integrated with the assumption that the luminescence is isotropic.

3. Results and discussion

The XRD patterns of the samples are presented in Fig. 1(a–d). The precursor glass is amorphous with diffuse humps. After crystallization, the XRD pattern shows intense diffraction peaks assigned to the orthorhombic β-YF_3 crystals (JCPDS no. 74-0911). The mean size of the crystals was calculated to be about 20 nm by the Scherrer formula. The TEM image of the nano-composite, shown in Fig. 1(e), demonstrates that the spherical YF_3 nano-crystals are distributed densely and homogeneously among the glassy matrix.

Fig. 2 shows the absorption spectra of the triply doped precursor glass and glass ceramic. The corresponding absorption bands of Ho^{3+}, Tm^{3+}, or Yb^{3+} are indexed in the figure. Apparently, the triply doping does not change the level positions of these ions. The Yb^{3+} has only one excited state ($^2F_{5/2}$) about 10,000 cm^{-1} above the ground state ($^2F_{7/2}$). It is worthwhile to mention that the crystal-like Stark splits of the absorption bands appear obviously in the glass ceramic due to the partition of RE ions into the precipitated YF_3 nano-crystals [21,22]. To analyze the variation of the optical absorption behavior after crystallization,

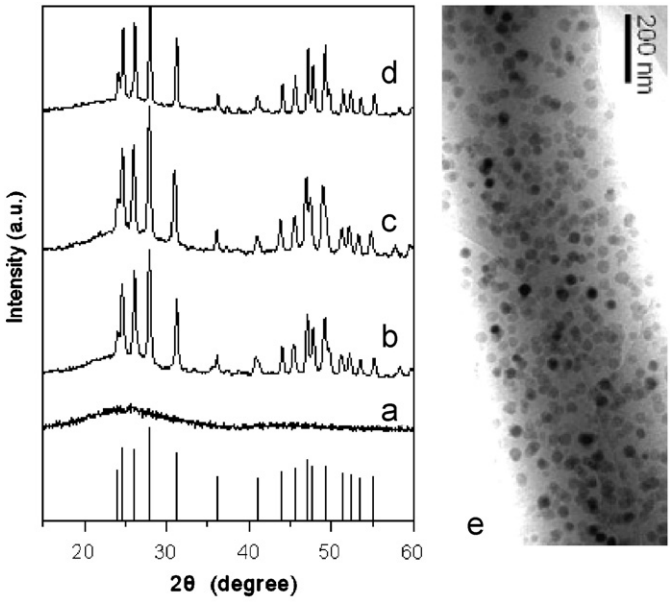

Fig. 1. XRD patterns of (a) the precursor glass, (b) 0.1TmF_3–0.5YbF_3, (c) 0.1HoF_3–0.5YbF_3 and (d) 0.1HoF_3–0.1TmF_3–0.5YbF_3-co-doped nano-composite, the bars represent the diffraction pattern of the standard β-YF_3 phase, (e) TEM micrograph of glass ceramic.

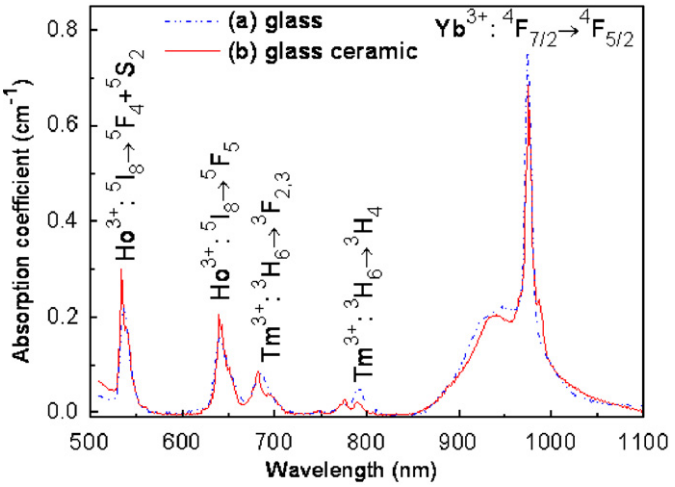

Fig. 2. Optical absorption spectra of (a) the precursor glass and (b) the glass ceramic doped with 0.2HoF_3–0.1TmF_3–0.5YbF_3.

Table 1
The calculated Judd–Ofelt parameters of Ho^{3+} and Tm^{3+} ions in the precursor glass and glass ceramic

Judd–Ofelt parameters (10^{-20} cm^{-1})	Glass		Glass ceramic	
	Ho^{3+}	Tm^{3+}	Ho^{3+}	Tm^{3+}
Ω_2	2.63	3.42	0.73	1.88
Ω_4	3.43	3.07	3.57	3.83
Ω_6	1.10	0.89	1.65	0.28

the Judd–Ofelt analysis [23–24] was carried out. Generally speaking, the intensity parameter Ω_2 is sensitive to the environmental configuration symmetry of the RE ions, and it decreases with the host changing from oxides to fluorides [25–28]. The results presented in Table 1 show that Ω_2 in the glass ceramic is much smaller than that in the precursor glass, indicating that some RE ions are incorporated into YF_3 nano-crystals. The partition of RE ions in the precipitated fluoride nano-phase has also been observed in other oxyfluoride glass ceramics [15–19].

The UC emission spectra of the Ho^{3+}/Yb^{3+}-co-doped precursor glass and glass ceramic are shown in Fig. 3(a). Both spectra exhibit intense green and weak red emission bands of Ho^{3+} originated from $^4S_2$, $^5F_4 \rightarrow {}^5I_8$ (~544 nm) and $^5F_5 \rightarrow {}^5I_8$ (~640 nm) transitions, respectively. In comparison with those of the precursor glass, both the green and red emissions of the glass ceramic are greatly intensified (to about 20 times for the green emission), and the obvious Stark splits of these emission bands are observed, further confirming the partition of RE ions into β-YF_3 nano-crystals with low phonon energy after crystallization. The excitation power dependence of the intensities of these emission signals, as shown in Fig. 3(c), exhibits a square relationship which indicates the participation of two pumping photons to populate the $^4S_2$, $^5F_4$ and $^5F_5$ levels through energy transfer (ET) from Yb^{3+} to Ho^{3+}. Firstly, Ho^{3+} ions are excited from the ground level $^5I_8$ to the $^5I_6$ level with the exceeding energy (~1600 cm^{-1}) transferred to the host matrix as optical phonons. After the Ho^{3+}:$^5I_6$ level is populated, Yb^{3+} absorbs a second photon and then transfers the energy to Ho^{3+}:$^4S_5$, $^5F_4$ thermalized emitting levels from which the green emission band at 544 nm arises. As for the red emission, there exist two possible energy ways for the population of Ho^{3+}:$^5F_5$ emitting level: (1) Yb^{3+}:$^2F_{5/2}$+Ho^{3+}:$^5I_7 \rightarrow Yb^{3+}$:$^2F_{7/2}$+$Ho^{3+}$:$^5F_5$ where $^5I_7$ level is populated through the non-radiative decay of

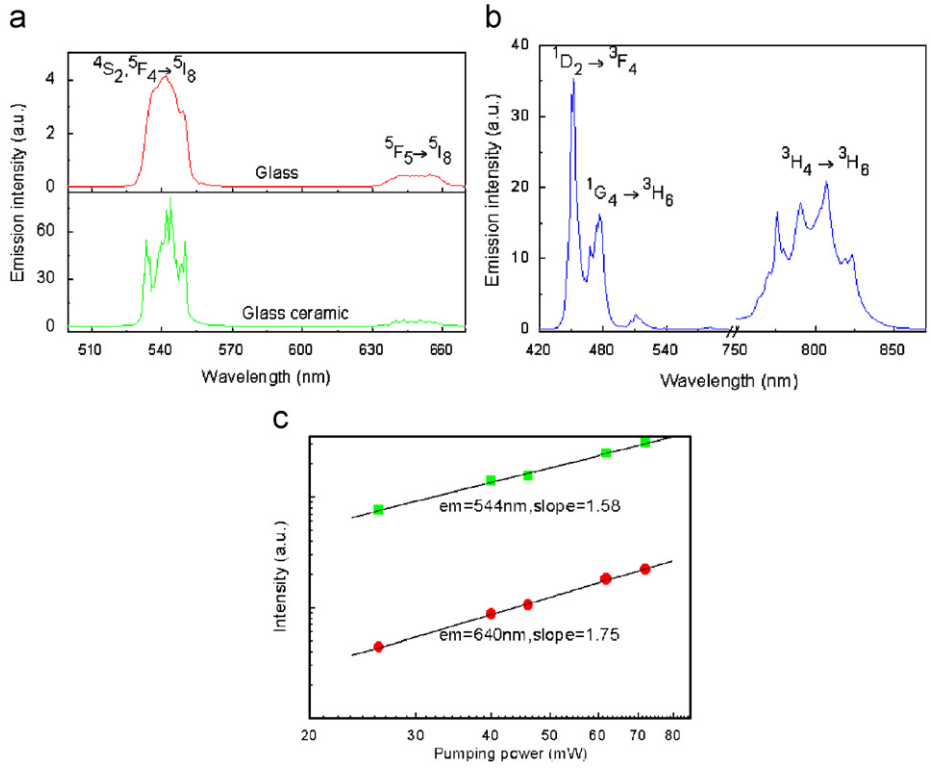

Fig. 3. Typical visible upconversion luminescence under 976 nm excitation from (a) the $0.1Ho^{3+}$–$0.5Yb^{3+}$-co-doped glass and glass ceramic, (b) the $0.1Tm^{3+}$–$0.5Yb^{3+}$-co-doped glass ceramic and (c) log–log plot of the upconversion emission intensity versus the pumping power for the $0.1Ho^{3+}$–$0.5Yb^{3+}$-co-doped glass ceramic.

$^5I_6$ level; (2) non-radiative phonon-assisted relaxation from the $^4S_2$, $^5F_4$ excited levels to the $^5F_5$ level. The UC luminescence of the Tm^{3+}/Yb^{3+}-co-doped glass ceramic is shown in Fig. 3(b). The intense blue emissions at 451 and 478 nm corresponding to Tm^{3+} $^1D_2 \rightarrow {}^3F_4$ and $^1G_4 \rightarrow {}^3H_6$ transitions, respectively, and the near-infrared emission at 790 nm owing to Tm^{3+} $^3H_4 \rightarrow {}^3H_6$ transition are detected. We proposed that the population of $^1G_4$ is accomplished by the three-step sequential ETs from the excited Yb^{3+} to Tm^{3+}, and the excitation of $^1D_2$ is a four-photon UC process assisted by the cross-relaxation between Tm^{3+} ions: $^3F_2+{}^3H_4 \rightarrow {}^3H_6+{}^1D_2$ [22]. The intense ultraviolet emissions at 346 and 362 nm corresponding to $^1I_6 \rightarrow {}^3F_4$ and $^1D_2 \rightarrow {}^3H_6$ transitions of Tm^{3+} are also recorded in this sample. The possible UC mechanisms for the Yb^{3+} sensitized Ho^{3+} or Tm^{3+} emissions in the glass ceramics are demonstrated in detail (Fig. 4).

In order to obtain the red luminescence, the UC emissions of $0.05Ho^{3+}/x Tm^{3+}/0.5Yb^{3+}$ triply doped glass ceramics were investigated. Remarkably, the introduction of Tm^{3+} into the nano-composite significantly influences the UC emissions of Ho^{3+}. With the increasing of Tm^{3+} content, the emission intensity ratio of red to green is monotonously enhanced, as shown in Fig. 5. The intensification of red luminescence is possibly ascribed to the efficient ET process between Tm^{3+} and Ho^{3+} concentrated in β-YF_3 nano-crystals (illustrated in Fig. 4): Ho^{3+}:$^5I_8$+Tm^{3+}:$^3F_4 \rightarrow$ Ho^{3+}:$^5I_7$+Tm^{3+}:$^3H_6$ [29–31]. Hereafter, the ET Yb^{3+}:$^2F_{5/2}$+Ho^{3+}:$^5I_7 \rightarrow Yb^{3+}$:$^2F_{7/2}$+$Ho^{3+}$:$^5F_5$ occurs to populate the Ho^{3+}:$^5F_5$ level from which the red emission band at 640 nm arises. The ET process for the population of the Ho^{3+}:$^5I_7$ level had already been identified as the origin of the 2.0 μm mid-infrared emissions in Ho^{3+}–Tm^{3+}-co-doped crystals and glasses [29–31]. The red emission is very weak in the Ho^{3+}/Yb^{3+}-co-doped glass ceramic, and it is significantly enhanced when Tm^{3+} is introduced to the system, indicating that the above-mentioned ET processes play a dominant role in populating the $^5F_5$ excited level of Ho^{3+}.

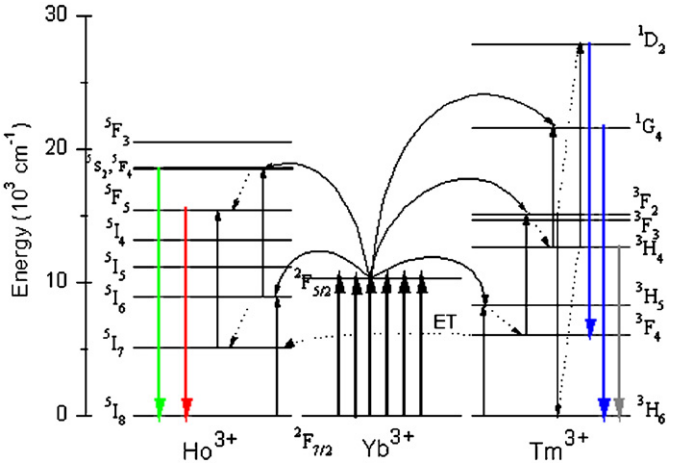

Fig. 4. Schematic diagram illustrating the mechanisms of Yb^{3+} sensitized Ho^{3+} or Tm^{3+} upconversion luminescence, and the energy transfers between Tm^{3+} and Ho^{3+}.

Based on the generation of red, green and blue emissions mentioned above, it is possible to obtain luminescence with a wide spectrum of colors, including white, by appropriate doping of Yb^{3+}, Tm^{3+} and Ho^{3+} in the nano-composite. Fig. 6 shows the UC emission spectra of the $x Ho^{3+}/0.1Tm^{3+}/0.5Yb^{3+}$ ($x = 0.01$, 0.02, 0.05, 0.1, 0.2) triply doped samples under 976 nm excitation. The primary red (Ho^{3+} $^5F_5 \rightarrow {}^5I_8$), green ($Ho^{3+}$ $^4S_2$, $^5F_4 \rightarrow {}^5I_8$) and blue ($Tm^{3+}$ $^1D_2 \rightarrow {}^3F_4$, $^1G_4 \rightarrow {}^3H_6$) emissions with controllable relative intensity by variation of RE doping content are simultaneously generated. For all the triply doped samples, the intensity of the red emission is far stronger than that of the Ho^{3+}/Yb^{3+}-co-doped ones, ascribing to the Tm^{3+} sensitizing effect on Ho^{3+}. On the other hand, the blue luminescence as well as the near infrared one

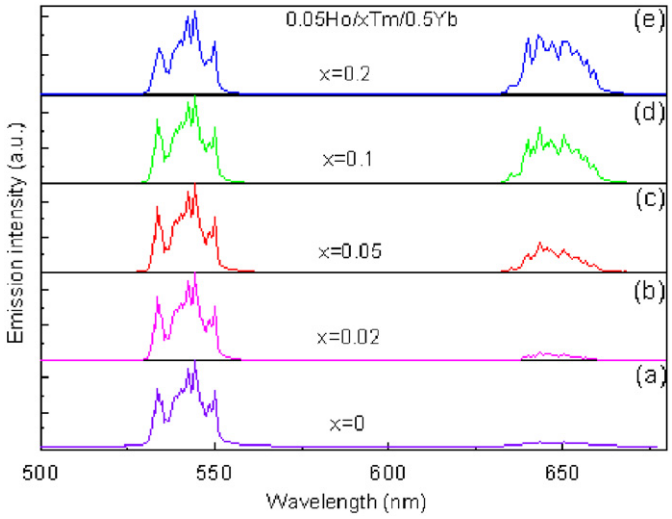

Fig. 5. Upconversion emission spectra from (a) $0.05Ho^{3+}/0Tm^{3+}/0.5Yb^{3+}$, (b) $0.05Ho^{3+}/0.02Tm^{3+}/0.5Yb^{3+}$, (c) $0.05Ho^{3+}/0.05Tm^{3+}/0.5Yb^{3+}$, (d) $0.05Ho^{3+}/0.1Tm^{3+}/0.5Yb^{3+}$ and (e) $0.05Ho^{3+}/0.2Tm^{3+}/0.5Yb^{3+}$ triply doped glass ceramics under 976 nm excitation.

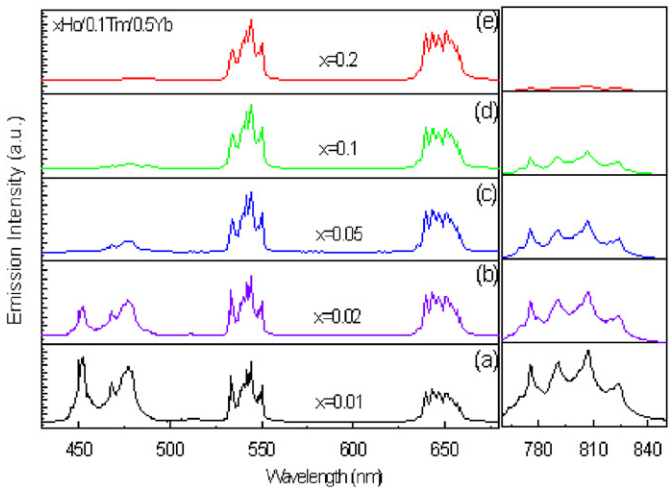

Fig. 6. Upconversion emission spectra from (a) $0.01Ho^{3+}/0.1Tm^{3+}/0.5Yb^{3+}$, (b) $0.02Ho^{3+}/0.1Tm^{3+}/0.5Yb^{3+}$, (c) $0.05Ho^{3+}/0.1Tm^{3+}/0.5Yb^{3+}$, (d) $0.1Ho^{3+}/0.1Tm^{3+}/0.5Yb^{3+}$ and (e) $0.2Ho^{3+}/0.1Tm^{3+}/0.5Yb^{3+}$ triply doped glass ceramics under 976 nm excitation. All the emissions are normalized to the green emission band.

assigned to Tm^{3+} $^3H_4 \rightarrow {}^3H_6$ transition are weakened with the increasing of Ho^{3+} content, attributing to the depopulation of Tm^{3+} $^3F_4$ excited level by the ETs from Tm^{3+} to Ho^{3+}, i.e., Ho^{3+}:$^5I_8$+Tm^{3+}:$^3F_4 \rightarrow Ho^{3+}$:$^5I_7$+$Tm^{3+}$:$^3H_6$. Therefore, by reasonable adjusting Ho^{3+}, Tm^{3+} and Yb^{3+} doping, the intense red, green and blue emissions with almost equal intensity are obtained in the $0.02Ho^{3+}/0.1Tm^{3+}/0.5Yb^{3+}$ triply doped nano-composite, which yields the bright white light clearly seen by the naked eyes, as shown in the inset of Fig. 7.

The UC emission spectra for the samples doped with various contents of Yb^{3+}, Tm^{3+} and Ho^{3+} are converted to the CIE 1931 chromaticity diagram and plotted in Fig. 7. For the $0.1Ho^{3+}/0.5Yb^{3+}$- and $0.1Tm^{3+}/0.5Yb^{3+}$-co-doped samples, the pure green and blue emissions are achieved, respectively; while for the $xHo^{3+}/0.1Tm^{3+}/0.5Yb^{3+}$ triply doped samples, the apparent luminescence is tuned sequentially to cyan, white and yellow with the variation of Ho^{3+} content (x) from 0.01, 0.02 to 0.05~0.2, respectively. The CIE coordinate of the $0.02Ho^{3+}/0.1Tm^{3+}/0.5Yb^{3+}$

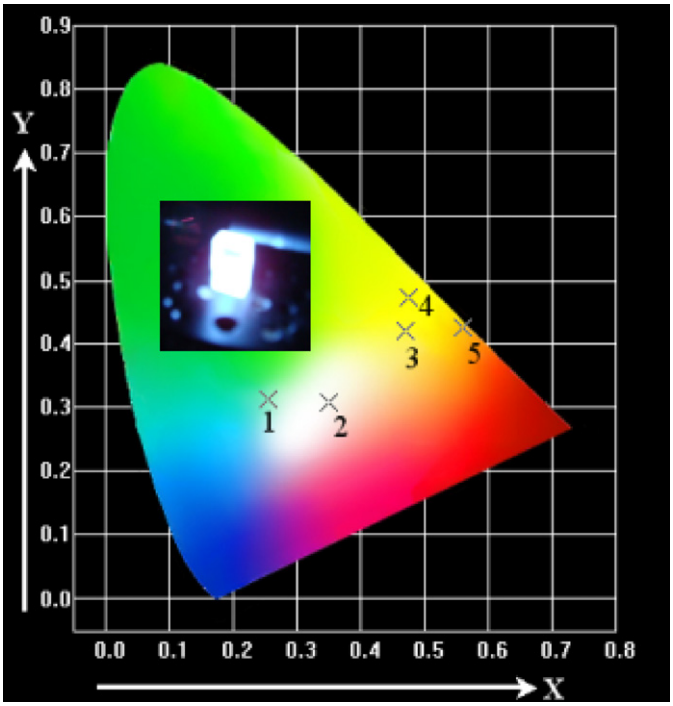

Fig. 7. CIE (X, Y) coordinate diagram showing the chromaticity points of the emissions in the xHo/0.1Tm/0.5Yb triply doped glass ceramics: (1) $x = 0.01$, (2) $x = 0.02$, (3) $x = 0.05$, (4) $x = 0.1$,and (5) $x = 0.2$; the inset shows the digital photo of the white-light emission from 0.02Ho/0.1Tm/0.5Yb triply doped glass ceramic.

triply doped glass ceramic ($X = 0.351$, $Y = 0.306$), shown by point 2 (white region) in Fig. 7, is very close to the standard equal energy white-light illumination ($X = 0.333$, $Y = 0.333$). Based on the spectroradiometer measurement, the UC white-light power of ~120 μW was estimated for the absorbed pump laser power of ~60 mW. Thus, the energy conversion efficiency, defined as the ratio between the UC emitting power and the absorbed pump laser power, is about 0.2%.

4. Conclusions

Novel nano-composites containing $Ho^{3+}/Tm^{3+}/Yb^{3+}$:β-YF_3 nano-crystals were successfully prepared. Bright white light with CIE-$X = 0.351$ and CIE-$Y = 0.306$ was generated through frequency UC under single 976 nm laser excitation. The red, green and blue signals, assigned to Ho^{3+} $^5F_5 \rightarrow {}^5I_8$, Ho^{3+} $^4S_2(^5F_4) \rightarrow {}^5I_8$ and Tm^{3+} $^1D_2 \rightarrow {}^3F_4$, $^1G_4 \rightarrow {}^3H_6$ transitions, respectively, were achieved via successive ET from Yb^{3+} to Ho^{3+} or Tm^{3+}. An absolute white-light power of ~120 μW was obtained for an absorbed pump laser power of ~60 mW. Such efficient white UC emission of the nano-composite makes it an excellent candidate applicable in the solid-state multicolor three-dimensional display.

Acknowledgments

This work was supported by the National Natural Science Foundation of China (50672098), the Major Science and Technology Project of Fujian Province (2005HZ01-1, 2007HZ0002-2), the National Engineering Research Center for Optoelectronic Crystalline Materials (2005DC105003), the Knowledge Innovation Program of the Chinese Academy of Sciences and the State Key Laboratory of Structural Chemistry (20080039).

References

[1] F. Auzel, C. R. Acad. Sci. 262 (1966) 1016.
[2] F. Auzel, Chem. Rev. 104 (2004) 139.
[3] R. Yan, Y. Li, Adv. Funct. Mater. 15 (2005) 763.
[4] Y. Sun, Y. Chen, L. Tian, Y. Yu, X. Kong, J. Zhao, H. Zhang, Nanotechnology 18 (2007) 275609.
[5] C.H. Liu, D.P. Chen, J. Mater. Chem. 17 (2007) 3875.
[6] E. Downing, L. Hesselink, J. Ralston, R. MacFarlane, Science 273 (1996) 1185.
[7] J.E.C. da Silva, G.F. de Sá, P.A. Santa-Cruz, J. Alloys Compd. 344 (2002) 260.
[8] H.T. Amorim, M.V.D. Vermelho, A.S. Gouveia-Neto, F.C. Cassanjes, S.J.L. Ribeiro, Y.J. Messaddeq, Solid State Chem. 171 (2003) 278.
[9] M. Liao, L. Hu, Y. Fang, J. Zhang, H. Sun, S. Xu, L. Zhang, Spectrochim. Acta A 68 (2007) 531.
[10] S. Xu, H. Ma, D. Fang, Z. Zhang, Z. Jiang, Mater. Lett. 59 (2005) 3066.
[11] J.E.C. Silva, G.F. de Sá, P.A. Santa-Cruz, J. Alloys Compd. 323–324 (2001) 336.
[12] D. Chen, Y. Wang, T. Guo, K. Zheng, Y. Yu, P. Huang, Appl. Phys. Lett. 91 (2007) 251903.
[13] A.S. Gouveia-Neto, L.A. Bueno, R.F. do Nascimento, E.A. da Silva Jr., E.B. da Costa, V.B. do Nascimento, Appl. Phys. Lett. 91 (2007) 091114.
[14] Y. Wang, J. Ohwaki, Appl. Phys. Lett. 63 (1993) 3268.
[15] D. Chen, Y. Wang, Y. Yu, E. Ma, L. Zhou, J. Solid State Chem. 179 (2006) 532.
[16] F. Liu, E. Ma, D. Chen, Y. Yu, Y. Wang, J. Phys. Chem. B 110 (2006) 20843.
[17] D. Chen, Y. Wang, Y. Yu, E. Ma, J. Solid State Chem. 179 (2006) 1445.
[18] L. Lahoz, S.E. Hernández, N.E. Capuj, D. Navarro-Urrios, Appl. Phys. Lett. 90 (2007) 201117.
[19] L. Huang, T. Yamashita, R. Jose, Y. Arai, T. Suzuki, Y. Ohishi, Appl. Phys. Lett. 90 (2007) 131116.
[20] C. Liu, J. Heo, Mater. Lett. 61 (2007) 3751.
[21] D. Chen, Y. Wang, E. Ma, Y. Yu, F. Liu, R. Li, J. Appl. Phys. 102 (2007) 023504.
[22] D. Chen, Y. Wang, Y. Yu, P. Huang, Appl. Phys. Lett. 91 (2007) 051920.
[23] B.R. Judd, Phys. Rev. 127 (1962) 750.
[24] G.S. Ofelt, J. Chem. Phys. 37 (1962) 511.
[25] E.W.J.L. Oomen, A.M.A. van Dongen, J. Non-Cryst. Solids 111 (1989) 205.
[26] X. Zou, T. Izumitani, J. Non-Cryst. Solids 162 (1993) 68.
[27] Y. Nageno, H. Takebe, K. Morinaga, T. Izumitani, J. Non-Cryst. Solids 169 (1994) 288.
[28] M. Bettinelli, A. Speghini, M. Ferrari, M. Montagna, J. Non-Cryst. Solids 201 (1996) 211.
[29] G. Özen, S. Salihoğlu, Opt. Commun. 180 (2000) 323.
[30] B.M. Walsh, N.P. Barnes, B. Di Bartolo, J. Lumin. 90 (2000) 39.
[31] V.A. French, R.R. Petrin, R.C. Powell, M. Kokta, Phys. Rev. B 46 (1992) 8018.